BiMLP: Compact Binary Architectures for Vision Multi-Layer Perceptrons

Yixing Xu, Xinghao Chen, Yunhe Wang
Huawei Noah's Ark Lab
{yixing.xu, xinghao.chen, yunhe.wang}@huawei.com

Abstract

This paper studies the problem of designing compact binary architectures for vision multi-layer perceptrons (MLPs). We provide extensive analysis on the difficulty of binarizing vision MLPs and find that previous binarization methods perform poorly due to limited capacity of binary MLPs. In contrast with the traditional CNNs that utilizing convolutional operations with large kernel size, fully-connected (FC) layers in MLPs can be treated as convolutional layers with kernel size 1×1. Thus, the representation ability of the FC layers will be limited when being binarized, and places restrictions on the capability of spatial mixing and channel mixing on the intermediate features. To this end, we propose to improve the performance of binary MLP (BiMLP) model by enriching the representation ability of binary FC layers. We design a novel binary block that contains multiple branches to merge a series of outputs from the same stage, and also a universal shortcut connection that encourages the information flow from the previous stage. The downsampling layers are also carefully designed to reduce the computational complexity while maintaining the classification performance. Experimental results on benchmark dataset ImageNet-1k demonstrate the effectiveness of the proposed BiMLP models, which achieve state-of-the-art accuracy compared to prior binary CNNs.

1 Introduction

Recent years have witness the boosting of convolutional neural networks (CNNs) on several computer vision (CV) applications, *e.g.* image recognition [21, 40, 17, 10, 14, 13], object detection [37, 36, 11, 9], semantic segmentation [34] and low-level vision [23, 32]. However, the success of CNN models highly depends on their huge computational cost and massive parameters, which are not suitable to be directly applied to edge devices that have limited computational resources such as mobile phones, smart watches and so on.

There are several model compression and acceleration methods to reduce the number of parameters and FLOPs of the original CNNs and derive a portable model. For instance, knowledge distillation [19, 49, 50] aims to train a small student network with the help of a cumbersome teacher network. Filter pruning [30, 18, 44, 43] methods sort the weights of the network based on their importance and throw away those who have negligible influence on the final performance. Model quantization [4, 56, 33] methods reduce the original 32-bit floating point weights and activations into lower bits and tensor decomposition [1, 47] methods express a large weight tensor as a sequence of elementary operations on a series of simpler tensors. Among them, binary CNN [55, 35, 15] is an extreme case of model quantization that uses only 1-bit for weights and activations. Compared to the original convolutional operation, binarized one has $64\times$ less FLOPs and $32\times$ less memory consumption.

Note that all of the existing binarization methods are applied on the convolutional operations in CNN models. However, multi-layer perceptron (MLP) model also shows its potential on CV tasks [45, 3, 12] and matrix multiplication is computational friendly to GPUs and has advantage on inference time

36th Conference on Neural Information Processing Systems (NeurIPS 2022).

in reality. Compared to traditional CNNs that utilize convolutional operation with various kernel sizes, FC layers in MLP models can be treated as convolutions with kernel size 1×1, which suffer more from limited representation ability compared to the convolutional operations with larger kernel size when being binarized. In fact, directly binarizing MLP models with the existing methods show more severe performance degradation compared to the CNN models. For example, the Top-1 classification accuracy on ImageNet will drop by more than 23% when binarizing CycleMLP [3] and WaveMLP [42] with the method proposed in Dorefa-Net [55] while the performance drop is only 17% for ResNet-18 [17] using 3×3 kernel size for most of the convolutional layers and 13% for AlexNet [21] with larger kernel size (11×11 and 5×5).

Thus, in order to alleviate the problem mentioned above, we introduce a novel binary block for MLP model that contains multiple branches to merge a series of outputs from the same stage of the network. Besides, a universal shortcut connection (Uni-shortcut) is designed to better transfer the knowledge from previous layers to the current layer. Compared to the original shortcut connection, the proposed Uni-shortcut can merge two features with different shapes. By fusing the outputs of multiple layers derived from the same or different stages of the network, we show that the representation power of the binary MLP is drastically increased. The downsampling layers are also modified to reduce the computational complexity while maintaining the classification performance. Experimental results on ImageNet-1k dataset demonstrate that by using the proposed method, we achieve state-of-the-art performance compared to other binary CNN models, as shown in Fig. 1.

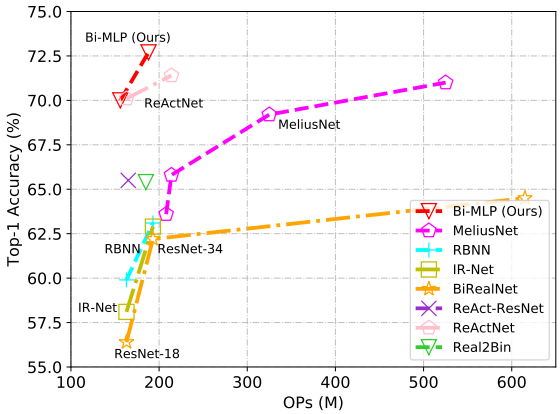

Figure 1: Accuracy vs. OPs of different binary models on ImageNet-1k dataset.

We summarize our contributions for learning 1-bit vision MLPs as follows:

- This paper points out the main difficulty of binarizing MLP models is that the representation ability of FC layers is worse than the convolutional layers in CNN models with kernel size larger than 1×1.
- We introduce a mulit-branch binary MLP block (MBB block) with Uni-shortcut operation to unlock the representation power of binary MLP models and also modify the architecture of downsampling layer to reduce the computational complexity.
- The experimental results on ImageNet-1k dataset show that the proposed BiMLP improves the top-1 accuracy by 1.3% with 12.1% less OPs compared to the state-of-the-art ReActNet, which indicates the effectiveness of the proposed BiMLP models.

2 Preliminaries

2.1 Binarization in CNN models

Given the weights $W \in \mathbb{R}^{c_o \times c_i \times k \times k}$ where c_i and c_o are the number of input and output channels and k is the kernel size, and also the activation $A \in \mathbb{R}^{c_i \times h \times w}$ where h and w are the height and width of the input feature, a common way of binarizing the weights and activations in CNN models is to apply sign function on the 32-bit floating point inputs, *i.e.*,

$$W_b = sign(W), \quad A_b = sign(A), \tag{1}$$

in which $sign(\cdot)$ is an element-wise operation that outputs +1 when the input is positive and -1 otherwise. Given the binarized weights and activations, the convolutional operation can be realized with binary operations only, *i.e.*:

$$Y = W_b \odot A_b, \tag{2}$$

in which $\odot$ represents binary convolutional operation that can be implemented with XNOR and POPCOUNT.

Note that the gradient of aforementioned sign function is zero almost everywhere and backward propagation is unable to be applied during training. Thus, the back-propagation of sign function follows the straight through estimator (STE) rule:

$$\frac{\partial \mathcal{L}}{\partial W} = Clip(\frac{\partial \mathcal{L}}{\partial W_b}, -1, 1), \tag{3}$$

where $\mathcal{L}$ is the loss function corresponding to the specific task, *e.g.*, cross-entropy loss for image classification. The $Clip(\cdot, -1, 1)$ function clips the elements of the gradient into range $[-1, 1]$.

Most of the existing binary CNN methods focus on improving the forward sign function and backward STE rule. For example, XNOR-Net [35] introduces channel-wise scale factors on the pure sign function and improves the performance of binary CNN. Dorefa-Net [55] uses only a single scale factor to achieve similar performance. ReActNet [27] proposes RSign and RPreLU function for binary CNNs. DSQ [8] replaces the STE rule and uses the gradient of tanh function to replace the gradient of sign function while BNN+ [6] introduces SignSwish function. Methods mentioned above are all applied on CNN models and directly transfer them to MLP models results in severe performance degradation.

2.2 Vision MLP Models

Vision MLP models take patches of image (tokens) as input, and stack a sequence of channel-FC layers and spatial-FC layers for image recognition. Specifically, given the input $X \in \mathbb{R}^{n \times d}$ in which n is the number of tokens and d is the number of channels in each token, the channel-FC layer fuses the channels in a single token and generate d' channels, *i.e.*,

$$\text{channel-FC}(X, W_c) = X \cdot W_c, \tag{4}$$

where $W_c \in \mathbb{R}^{d \times d'}$ is the parameter matrix of the channel-FC layer, and $\cdot$ represents the matrix multiplication operation. Channel-FC layer only aggregates information from different input channels, while lacking the communications between tokens. Thus, the spatial-FC layer is also introduced in MLP models [45], *i.e.*,

$$\text{spatial-FC}(X, W_s) = W_s^\top \cdot X, \tag{5}$$

where $W_s \in \mathbb{R}^{n \times n'}$ is the parameter of spatial-FC layer. In general, MLP models usually set $d = d'$ and $n = n'$ to pursuit efficiency on both feature representation and computation of the entire network.

The spatial-FC layer mentioned above cannot deal with images with diverse shapes, thus is unable to be applied on downstream tasks such as image detection and image segmentation. In order to solve the problem, Cycle-MLP [3] retains the position of each token and introduces Cycle-FC layer to enlarge the receptive field of MLP to cope with downstream tasks while maintaining the computational complexity. Specifically, given the input feature $Z \in \mathbb{R}^{H \times W \times C_{in}}$, the output of Cycle-FC layer is:

$$\text{Cycle-FC}(Z)_{i,j,:} = \sum_{c=0}^{C_in} Z_{i+\delta_i(c), j+\delta_j(c), c} \cdot W^{cycle}_{c,:}; \tag{6}$$

in which $W^{cycle} \in \mathbb{R}^{C_{in} \times C_{out}}$ is the parameter matrix of the Cycle-FC layer, and $\delta_i(c)$ and $\delta_j(c)$ are defined as:

$$\delta_i(c) = (c \mod S_H) - 1, \qquad \delta_j(c) = (\lfloor \frac{c}{S_H} \rfloor \mod S_W) - 1, \tag{7}$$

where S_H and S_W are predefined receptive fields. Besides Cycle-MLP, Wave-MLP [42] represents token as a wave function with amplitude and phase and proposes Wave-FC layer to solve the above problem. AS-MLP [24] avoids the restriction of fixed input size by axially shifting channels of the feature map, and is able to obtain information flow from different axial directions.

Compared to the convolutional operation in CNN and self-attention operation in Transformer, matrix multiplication in MLP is computational friendly to GPUs and has specific advantage on inference time in reality. Benefits from its simple architecture, MLP models can be generalized to various hardware. However, the cumbersome MLP model with a large number of parameters and FLOPs limits its ability to apply to portable devices, which means it is essential to derive a compact MLP model, *e.g.* binary vision MLPs.

3 Binary Vision MLPs

In this section, we first analyze the difficulty of binarizing vision MLP through comparing the representation ability of binary features in FC layers and convolutional layers. We then propose a novel binary architecture for vision MLP, which fuses the outputs from the same layer with multi-branch MLP block and those from different layers with a universal shortcut connection to strengthen the representation ability of MLP.

3.1 Difficulty of Binarizing Vision MLP

Given the input feature $F \in \mathbb{R}^{C_{in} \times H \times W}$ and the convolutional kernel $K \in \mathbb{R}^{C_{out} \times C_{in} \times K_h \times K_w}$ in which K_h and K_w are the height and width of the kernel, respectively. The **computational complexity** of the convolutional operation is:

$$\mathcal{O}(C_{in} \times C_{out} \times K_h \times K_w \times H \times W). \tag{8}$$

After binarizing the weights and activations, the elements of the output feature map Y is derived from the following equation:

$$Y(o,i,j) = \sum_{c=1}^{C_{in}} \sum_{d_x=-\lfloor \frac{K_w}{2} \rfloor}^{\lfloor \frac{K_w}{2} \rfloor} \sum_{d_y=-\lfloor \frac{K_h}{2} \rfloor}^{\lfloor \frac{K_h}{2} \rfloor} F^b(c, i+d_y, j+d_x) \times K^b(o, c, d_y + \frac{K_h}{2}, d_x + \frac{K_w}{2}), \tag{9}$$

in which K^b and F^b are binarized kernel and input feature using Eq. 1 whose elements are selected from $\{+1, -1\}$. According to Eq. 9, we can easily conclude that each element in Y is chosen from $N+1$ different values from the set $S_b = \{-N, -N+2, ..., N-2, N\}$, in which $N = C_{in} \cdot K_h \cdot K_w$. Specifically, we denote the number N as the **representation ability** of the binary FC layer.

In traditional CNN models such as ResNet [17] and VGGNet [40], convolutional operation with kernel size 3×3 occupies the network. Efficient-Net [41] uses convolution with kernel size 3×3 and 5×5, while the recently proposed RepLKNet [7] expands the kernel size to 31×31. Different from the CNN models mentioned above, FC layers in MLP model can be treated as convolutional operation with kernel size 1×1.

Therefore, compared to the convolutional layer with kernel size $k \times k$, FC layer with the same number of input channels and output channels has $1/k^2$ computational complexity and $1/k^2$ representation ability after being binarized. Note that assuming CNN models and MLP models have the same number of input channels and output channels is reasonable. For example, WaveMLP-S [42] with $30M$ parameters and $4.5G$ FLOPs has four stages with base channel 64-128-320-512, while ResNet-50 with $25.5M$ parameters and $4.1G$ FLOPs has four stages with base channel 64-128-256-512 which are roughly the same.

In order to achieve the same representation ability as convolutional layer, the number of input channels of FC layer must be multiplied by k^2. Similarly, the number of output channels should also be scaled up in order to maintain the representation ability of the next FC layer. Hence, the computational complexity is k^2 times compared to the convolutional layer with kernel size $k \times k$, which drastically reduce the advantage of binary neural network. To this end, we design a novel binary architecture for vision models (BiMLP) to enhance the representation ability while maintaining compact model complexity. A series of specific design are proposed to achieve this goal, which will be elaborated in the following sections.

3.2 BiMLP Architecture

To deal with the above problem, we introduce a mulit-branch binary MLP block (MBB block) with Uni-shortcut operation to enhance the representation capacity of binary MLP models. We also design a novel architecture of downsampling layer for binary MLPs to further reduce the computational complexity while maintaining the accuracy.

Multi-branch binary MLP block. To enhance the representation ability of binary vision MLPs with compact complexity, we propose a new binary MLP block containing multiple branches. Note that in MLP-Mixer [45], ResMLP [46] and gMLP [54], an MLP block mainly consists of two parts including

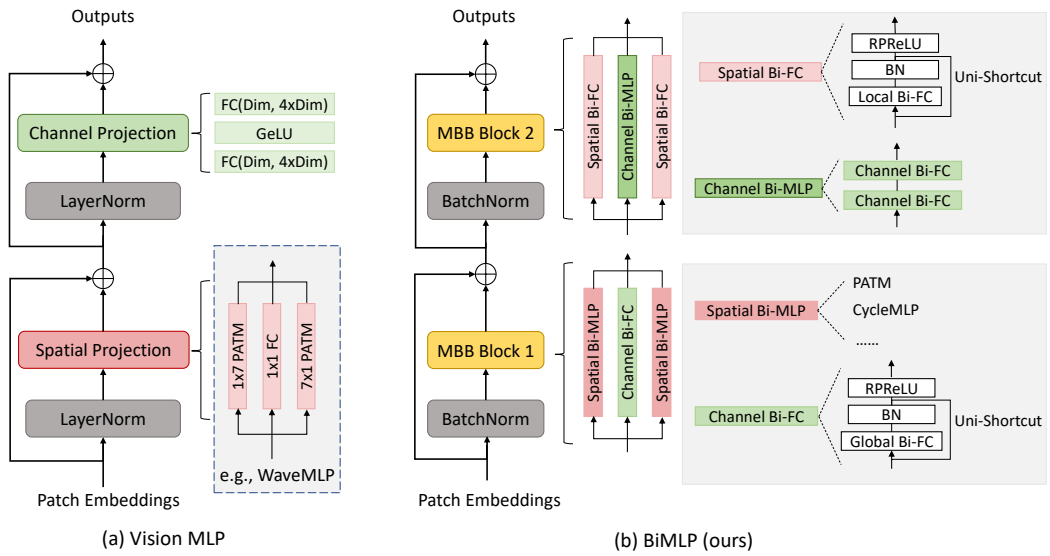

Figure 2: (a) Details of vision MLP blocks, *e.g.*, WaveMLP [42]. (b) The proposed Multi-branch binary MLP (MBB) blocks for BiMLP.

the spatial projection part and the channel projection part. For CycleMLP [3] and WaveMLP [42], the spatial projection is achieved by introducing some **local FC** operations (*e.g.* Cycle-FC, Wave-FC) which are applied on the adjacent tokens to cope with input images with different shapes. Meanwhile, the **global FC** layer (ordinary FC layer) is used for channel mixing. Different from them, we simultaneously introduce spatial projection and channel projection into a single part, and form two different multi-branch binary MLP blocks (MBB blocks) as shown in Fig. 2.

There are four different elements in the MBB blocks, *i.e.*, the Spatial Binary FC, the Spatial Binary MLP, the Channel Binary FC and the Channel Binary MLP. Given the binarized input feature X^b, the output of Spatial Binary FC is:

$$Y_{SB_FC} = \text{RPReLU}(\text{LFC}(\text{BN}(X^b)) + U(X^b)), \tag{10}$$

in which RPReLU$(\cdot)$ is the activation function introduced in ReActNet [27]. LFC$(\cdot)$ is the local FC that fuses the spatial information which is realized with different form in previous works. BN$(\cdot)$ is the ordinary batch normalization, and U$(\cdot)$ is the proposed Uni-shortcut which will be introduced below in Eq. 12. For Spatial Binary MLP, we utilize the PATM architecture introduced in WaveMLP [42]. Other forms such as CycleMLP architecture in [3], and axially shifting architecture in AS-MLP [24] can be used as a replacement.

The Channel Binary FC is defined as:

$$Y_{CB_FC} = \text{RPReLU}(\text{GFC}(\text{BN}(X^b)) + U(X^b)), \tag{11}$$

in which GFC$(\cdot)$ is the original global FC layer that mixes the information between different channels. Finally, the Channel Binary MLP is the stack of multiple Channel Binary FCs to strengthen the ability of channel mixing.

Given the four different elements introduced above, the first MBB block uses two Spatial Binary MLPs focusing on the height and width of the spatial dimension, and a Channel Binary FC. The second MBB block uses two Spatial Binary FC and a Channel Binary MLP. In this way, the channel projection and spatial projection are used multiple times, while at the same time the first block has a stronger ability for spatial mixing and the second block is good at mixing the channel information. Finally, all the layer normalizations are replaced with batch normalizations, as shown in the ablation study in Tab. 4.

With the above architectures, the representation ability can be recovered with less computational complexity by using multiple branches compared with directly expanding the input and output channels. Generally, k^2 branches are needed to get the same representation ability, and the computational complexity is the same compared to the convolutional layer with kernel size $k \times k$. Note that as

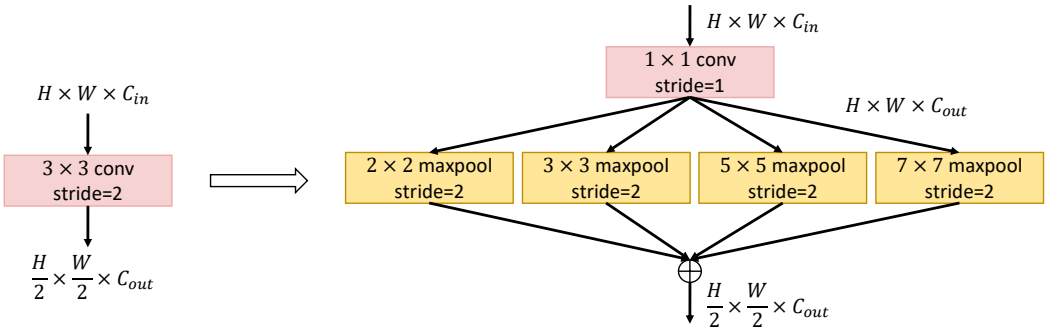

Figure 3: Left: The original downsampling layer used in 32-bit floating point MLP models. Right: The proposed downsampling block for BiMLP.

the number of branches increases, both the representation ability and the computational complexity will increase. Thus, we seek for a balance between the effectiveness and the efficiency. In the following experiments, we use only 3 branches as mentioned above and show that it is enough to obtain competitive results in Tab. 3.

Uni-shortcut. Recall that the proposed MBB blocks fuse the information from the same layer. The previous works of binary CNNs show that combining the outputs from different layers is important for the information flow. However, the number of output channels and input channels are usually different in MLP models and the original shortcut connection cannot be directly applied. Since the input channels c_{in} are usually multiple times of the output channels c_{out} (or vise versa), *i.e.* $c_{in} = nc_{out}$ (or $c_{out} = nc_{in}$), $n \in N^+$. Therefore, we propose a universal shortcut (Uni-shortcut) to cope with the following two different situations.

Given the input feature $X^b \in \mathbb{R}^{C_{in} \times H \times W}$ and a FC layer with c_{in} and c_{out} input and output channels, we have:

$$U(X^b) = \begin{cases} \frac{1}{n} \sum_{i=1}^{n} X^b(:,:, \frac{i-1}{n} c_{in} : \frac{i}{n} c_{in}), & c_{in} = nc_{out}, \\ concat(\sum_{i=1}^{n} X^b, \ dim = 2), & c_{out} = nc_{in}, \end{cases} \tag{12}$$

where the input is averaged based on the channel dimension when $c_{in} = nc_{out}$, and the input is repeated n times and concatenated together to fit the output dimension when $c_{out} = nc_{in}$.

Downsampling block. The downsampling layers are not binarized during training and inference for MLP models, otherwise the performance will drastically decrease, as also discussed in prior binary CNNs [28, 27, 35]. This brings the problem that the FLOPs of downsampling layers occupy the whole network since the 3×3 convolution with stride 2 is a common way of simultaneously reducing the spatial size and changing the number of channels of the feature maps. Thus, similar to [16], we separately handle the spatial and channel dimension by using 1×1 convolution with stride 1 (FC layer), and maxpooling with diverse kernel size to replace the original convolution, as shown in Fig. 3. By this way, the computational complexity is significantly reduced while the classification performance is maintained.

4 Experiments

In this section, we first evaluate the effectiveness of the proposed method on ImageNet dataset. The experimental settings include the dataset statistics, details of the network architectures and the training strategy is introduced in Sec. 4.1. In Sec. 4.2, we compare our method with a series of state-of-the-art binary CNN models in terms of accuracy and FLOPs. The ablation study on each part of the proposed method is conducted in Sec. 4.3.

Table 1: Details of different architectures of BiMLP. The parameter 'dim' indicates the dimension of features, and 'ratio' is the expand ratio of the mid layer of MLP. FLOPs is calculated on the layers that are not binarized, BOPs is calculated on binarized layer and OPs = BOPs / 64 + FLOPs. The computational complexity is calculated based on the input shape 224×224.

	Output size	BiMLP-S	BiMLP-M
Stage 1	$\frac{H}{4} \times \frac{W}{4}$	$\begin{bmatrix} \text{dim} = 64 \\ \text{ratio} = 4 \end{bmatrix} \times 2$	$\begin{bmatrix} \text{dim} = 64 \\ \text{ratio} = 4 \end{bmatrix} \times 2$
Stage 2	$\frac{H}{8} \times \frac{W}{8}$	$\begin{bmatrix} \text{dim} = 128 \\ \text{ratio} = 4 \end{bmatrix} \times 2$	$\begin{bmatrix} \text{dim} = 128 \\ \text{ratio} = 4 \end{bmatrix} \times 3$
Stage 3	$\frac{H}{16} \times \frac{W}{16}$	$\begin{bmatrix} \text{dim} = 320 \\ \text{ratio} = 4 \end{bmatrix} \times 4$	$\begin{bmatrix} \text{dim} = 320 \\ \text{ratio} = 4 \end{bmatrix} \times 10$
Stage 4	$\frac{H}{32} \times \frac{W}{32}$	$\begin{bmatrix} \text{dim} = 512 \\ \text{ratio} = 4 \end{bmatrix} \times 2$	$\begin{bmatrix} \text{dim} = 512 \\ \text{ratio} = 4 \end{bmatrix} \times 3$
FLOPs ($\times 10^8$)		1.21	1.21
BOPs ($\times 10^9$)		2.25	4.32
OPs ($\times 10^8$)		1.56	1.88

Table 2: Experimental results on ImageNet-1k using different binary CNN models and the proposed BiMLP. Bit-width (W/A) indicates the bit length of weights and activations. FLOPs is calculated on the full-precision layers, BOPs is calculated on binarized layers and OPs = BOPs / 64 + FLOPs.

Methods	Bit-width (W/A)	FLOPs ($\times 10^8$)	BOPs ($\times 10^9$)	OPs ($\times 10^8$)	Top-1 Acc (%)	Top-5 Acc (%)
XNOR-Net [35]	1/1	1.41	1.70	1.67	51.2	73.2
Dorefa-Net [55]	1/1	-	-	-	52.5	67.7
ABCNet [26]	1/1	-	-	-	42.7	67.6
Bireal-Net-18 [28]	1/1	1.39	1.68	1.63	56.4	79.5
Bireal-Net-34 [28]	1/1	1.39	3.53	1.93	62.2	83.9
UAD-BNN-18 [20]	1/1	-	-	-	57.2	80.2
UAD-BNN-34 [20]	1/1	-	-	-	62.8	84.5
RBNN-18 [25]	1/1	-	-	-	59.9	81.9
RBNN-34 [25]	1/1	-	-	-	63.1	84.4
Real2bin [31]	1/1	1.56	1.68	1.83	65.4	86.2
ReCU [51]	1/1	-	-	-	66.4	86.5
FDA-BNN [48]	1/1	-	-	-	66.0	86.4
LCR-BNN-18 [39]	1/1	-	-	-	59.6	81.6
LCR-BNN-34 [39]	1/1	-	-	-	63.5	84.6
LCR-BNN-ReAct [39]	1/1	-	-	-	69.8	85.7
Bi-half-18 [22]	1/1	-	-	-	60.40	82.86
Bi-half-34 [22]	1/1	-	-	-	64.17	85.36
MeliusNet-22 [2]	1/1	1.35	4.62	2.08	63.6	84.7
MeliusNet-29 [2]	1/1	1.29	5.47	2.14	65.8	86.2
MeliusNet-42 [2]	1/1	1.74	9.69	3.25	69.2	88.3
MeliusNet-59 [2]	1/1	2.45	18.3	5.25	71.0	89.7
ReActNet-B [27]	1/1	0.44	4.69	1.63	70.1	-
ReActNet-C [27]	1/1	1.40	4.69	2.14	71.4	-
BiMLP-S (Ours)	1/1	1.21	2.25	**1.56**	**70.0**	**89.6**
BiMLP-M (Ours)	1/1	1.21	4.32	**1.88**	**72.7**	**91.1**

4.1 Experimental Settings

ImageNet dataset. The benchmark dataset ImageNet-1k [38] contains over $1.2M$ training images and $50k$ validation images from 1,000 different categories. This is the most commonly used image classification dataset in other binary CNN methods.

Network architecture. We utilize the architecture proposed in [42] and replace the MLP block with the proposed MBB block with Uni-shortcut (Fig. 2(b)) as well as the replacement of downsampling blocks (Fig. 3). Details of the architectures of BiMLP models are specified in Tab. 1.

Table 3: Experimental results of using different branches in MBB blocks. The experiments are conducted using BiMLP-S model on ImageNet-1k dataset, and setting 3 is used as the baseline architecture which is the same as Fig. 2(b).

Setting	MBB Block 1		MBB Block 2		OPs	Top-1 Acc
	$\#S_1$	$\#C_1$	$\#S_2$	$\#C_2$	($\times 10^8$)	(%)
1	4	0	0	2	1.60	69.2
2	0	2	4	0	1.53	68.9
3	2	1	2	1	1.56	70.0
4	4	1	2	2	1.86	70.8
5	2	2	4	1	1.78	70.5

Training details. Following prior methods [28, 27, 31], we use a two step training strategy. In the first training step, we use the full precision MLP model as the teacher model and the network with the same architecture but binary activations as the student model. A knowledge distillation loss is used to facilitate the training of student network:

$$L = \alpha \sum_{i=1}^{n} L_{kl}(\mathbf{y}_s, \mathbf{y}_t) + (1-\alpha) \sum_{i=1}^{n} L_{ce}(\mathbf{y}_s, \mathbf{y}_{gt}), \tag{13}$$

in which $L_{kl}(\cdot)$ and $L_{ce}(\cdot)$ are the KL divergence and cross-entropy loss, $\mathbf{y}_s$ and $\mathbf{y}_t$ are the output probability of the student and teacher model, $\mathbf{y}_{gt}$ is the one-hot ground-truth probability and α is the trade-off hyper-parameter ($\alpha = 0.9$ in the following experiments). For the second training step, the full precision ResNet-34 is used as the teacher network. The binarized MLP model (both weights and activations) is used as the student model and the corresponding weights are initialized by the training results from the first step.

In both steps, the student models are trained for 300 epochs using AdamW [29] optimizer with momentum of 0.9 and weight decay of 0.05. We start with the learning rate of 1×10^{-3} and a cosine learning rate decay scheduler is used during training. We use NVIDIA V100 GPUs with a total batchsize of 1024 to train the model. The commonly used data-augmentation strategies such as Cut-Mix [52], Mixup [53] and Rand-Augment [5] are used. The first layer, the last layer and the downsampling layers are not binarized during training and inference.

4.2 Experimental Results on ImageNet

In this section, we compare the proposed model with the binary CNN models derived from other state-of-the-art methods on the ImageNet-1k dataset, including Dorefa-Net [55], XNOR-Net [35], ABCNet [26], Bireal-Net [28], Real2bin [31], MeliusNet [2], ReActNet [27], *etc.* As shown in Tab. 2, the proposed BiMLP models achieve competitive performance compared to the state-of-the-art binary CNN models. We can see that BiMLP-S achieves 70.0% top-1 accuracy and 89.6% top-5 accuracy with 0.156G OPs, which surpasses the most recent methods such as MeliusNet-42 by 0.8% and 1.3% with less than a half OPs, and is comparable to ReActNet-B. Meanwhile, BiMLP-M achieves 72.7% top-1 accuracy and 91.1% top-5 accuracy with only 0.188G OPs, which has 12.1% less OPs than ReActNet-C and is 1.3% better on top-1 accuracy. The above results show the superiority of the proposed BiMLP.

4.3 Ablation Studies

In this section, we demonstrate the effectiveness of each part of the proposed method by conducting a series of ablation studies.

Different branches in MBB blocks. Firstly, we show the experimental results of using different branches in Tab. 3. The $\#S_i$ indicates the number of Spatial Binary FC (MLP) in the MBB block i and $\#C_i$ is the number of Channel Binary FC (MLP) in the corresponding block. Note that we fuse the information along height and width of the feature map with different Spatial Binary FC (MLP), thus the $\#S_i$ should be even numbers. During the ablation study we keep $(\#S_1 + \#S_2)/(\#C_1 + \#C_2) = 2$ so that the ability of fusing information of different dimensions is roughly the same.

Table 4: Different forms of normalization layer and activation function. The experiments are conducted using BiMLP-S model on ImageNet-1k dataset.

Normalization	LN	LN	LN	LN	BN	BN	BN	BN
Activation	GeLU	ReLU	PReLU	RPReLU	GeLU	ReLU	PReLU	RPReLU
Top-1 Acc (%)	68.2	67.8	68.4	69.2	68.5	68.1	69.4	**70.0**

Table 5: Experimental results of using different form of residual connections. The experiments are conducted on ImageNet-1k dataset with BiMLP-S model.

	Top-1 Acc (%)
w/o shortcut	68.3
w/ Uni-shortcut	**70.0**
w/ shortcut	69.1

Table 6: Results of using different downsampling layers. 'Original' indicates the 3×3 convolution with stride 2, and 'proposed' means the proposed downsampling block as shown in Fig. 3 right.

Setting	OPs ($\times 10^8$)	Top-1 Acc (%)
Original	2.65	70.3
Proposed	1.56	70.0

The experiments are conducted on BiMLP-S model. As shown in Tab. 3, when the MBB blocks focus on only one dimension in setting 1 and 2, the top-1 accuracy decreases from 70.0% to 69.2% and 68.9%, which shows that mixing the information from different dimensions in a single block is important. In setting 4 and 5, more branches are used in each block compared to setting 3 (baseline), and only improves the accuracy by 0.8% and 0.5%, while increases 19.2% and 14.1% OPs. Thus, we use setting 3 for all the experiments considering the balance between the effectiveness and efficiency.

Normalization and activation. Different forms of normalization layer and activation function are compared. The candidates of normalization layer include Layer normalization (LN) and batch normalization (BN), and the candidates of activation functions are GeLU, ReLU, PReLU and RPReLU. As the results shown in Tab. 4, the combination of BN and RPReLU achieves the best accuracy, and is applied to all other experiments.

Shortcut connection. We also study the effectiveness of the proposed Uni-shortcut. Three different setting are used in this ablation study. The first is using the MBB block without any residual connection. The second is using the proposed Uni-shortcut in MBB blocks. The third is using the traditional shortcut in MBB blocks. In this circumstances, only those input-output pairs who have the same shape will be connected.

As shown in Tab. 5, compared to the MBB block without using any residual connection and using the traditional shortcut, Uni-shortcut improves the top-1 accuracy by 1.7% and 0.9% which shows the priority of the proposed method.

Downsampling layer. We compare the proposed downsampling block using the FC layer together with multi-branch maxpooling to the original downsampling layer using 3×3 convolution with stride 2 in Tab. 6. The result shows that we can significantly reduce the computational complexity from 0.265G to 0.156G (41.1% decrease) with only 0.3% drop of top-1 classification accuracy.

Hyper-parameters. As shown in Eq. 13, α is used as a hyper-parameter to balance the loss function between learning from the output probability of teacher model and learning from the ground-truth one-hot label. We report the accuracy on ImageNet-1k validation set in Fig. 4 and show that $\alpha = 0.9$ yields the best result.

Comparisons of different binarization methods. Finally, we compare the proposed method to other binarization methods proposed for CNN models in Tab. 7. The 1-bit model is to directly binarize the fp32 WaveMLP model using the sign function and the STE rule. The experimental results show that our method can significantly outperform other binarization methods that are directly applied to MLP model.

5 Conclusion

In this paper, we propose a new paradigm with specific architecture design for binarizing the vision MLP models. We point out that compared to binarizing the convolutional operation with large kernel

Table 7: Results of using different binarization methods on ImageNet-1k dataset. The 'FP32' model indicates the WaveMLP model, and '1-bit' model uses sign function and STE rule to binarize the FP32 model.

Model	Top-1 Acc(%)
FP32	80.1
1-bit	55.3
+ Dorefa-Net [55]	58.4
+ XNOR-Net [35]	59.1
+ ReActNet [27]	63.2
+ Ours	**70.0**

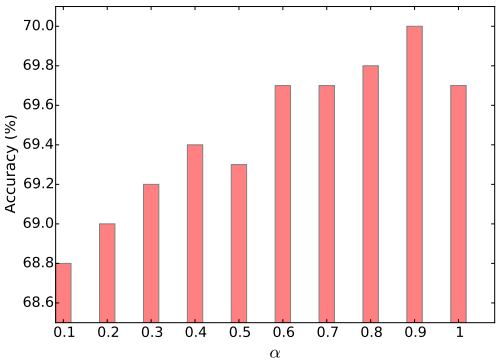

Figure 4: Top-1 acc vs. α on ImageNet val set.

size in CNN models, binarizing the FC layers yields a MLP model with poor representation ability. Simply increase the number of channels will fix this problem, but the computational complexity is quadratically increased. Thus, we propose a novel multi-branch binary MLP block (MBB block) with universal shortcut (Uni-shortcut) that can recover the representation ability while maintaining the computational complexity. We also redesign the downsampling layer that can significantly reduce the OPs of the binary MLP model while at the same time keep the performance roughly unchanged. The experimental results on ImageNet-1k dataset demonstrate the effectiveness of the proposed method, and we achieve a comparable performance with the state-of-the-art binary CNN models.

References

[1] Davide Bacciu and Danilo P Mandic. Tensor decompositions in deep learning. *arXiv preprint arXiv:2002.11835*, 2020.

[2] Joseph Bethge, Christian Bartz, Haojin Yang, Ying Chen, and Christoph Meinel. Meliusnet: Can binary neural networks achieve mobilenet-level accuracy? *arXiv preprint arXiv:2001.05936*, 2020.

[3] Shoufa Chen, Enze Xie, Chongjian Ge, Ding Liang, and Ping Luo. Cyclemlp: A mlp-like architecture for dense prediction. *arXiv preprint arXiv:2107.10224*, 2021.

[4] Brian Chmiel, Ron Banner, Gil Shomron, Yury Nahshan, Alex Bronstein, Uri Weiser, et al. Robust quantization: One model to rule them all. *Advances in neural information processing systems*, 33:5308–5317, 2020.

[5] Ekin D Cubuk, Barret Zoph, Jonathon Shlens, and Quoc V Le. Randaugment: Practical automated data augmentation with a reduced search space. In *Proceedings of the IEEE/CVF Conference on Computer Vision and Pattern Recognition Workshops*, pages 702–703, 2020.

[6] Sajad Darabi, Mouloud Belbahri, Matthieu Courbariaux, and Vahid Partovi Nia. Bnn+: Improved binary network training. 2018.

[7] Xiaohan Ding, Xiangyu Zhang, Yizhuang Zhou, Jungong Han, Guiguang Ding, and Jian Sun. Scaling up your kernels to 31x31: Revisiting large kernel design in cnns. *arXiv preprint arXiv:2203.06717*, 2022.

[8] Ruihao Gong, Xianglong Liu, Shenghu Jiang, Tianxiang Li, Peng Hu, Jiazhen Lin, Fengwei Yu, and Junjie Yan. Differentiable soft quantization: Bridging full-precision and low-bit neural networks. In *Proceedings of the IEEE/CVF International Conference on Computer Vision*, pages 4852–4861, 2019.

[9] Jianyuan Guo, Kai Han, Yunhe Wang, Han Wu, Xinghao Chen, Chunjing Xu, and Chang Xu. Distilling object detectors via decoupled features. In *Proceedings of the IEEE/CVF Conference on Computer Vision and Pattern Recognition*, pages 2154–2164, 2021.

[10] Jianyuan Guo, Kai Han, Han Wu, Yehui Tang, Xinghao Chen, Yunhe Wang, and Chang Xu. Cmt: Convolutional neural networks meet vision transformers. In *Proceedings of the IEEE/CVF Conference on Computer Vision and Pattern Recognition*, pages 12175–12185, 2022.

[11] Jianyuan Guo, Kai Han, Han Wu, Chao Zhang, Xinghao Chen, Chunjing Xu, Chang Xu, and Yunhe Wang. Positive-unlabeled data purification in the wild for object detection. In *Proceedings of the IEEE/CVF Conference on Computer Vision and Pattern Recognition*, pages 2653–2662, 2021.

[12] Jianyuan Guo, Yehui Tang, Kai Han, Xinghao Chen, Han Wu, Chao Xu, Chang Xu, and Yunhe Wang. Hire-mlp: Vision mlp via hierarchical rearrangement. In *Proceedings of the IEEE/CVF Conference on Computer Vision and Pattern Recognition*, pages 826–836, 2022.

[13] Kai Han, Yunhe Wang, Jianyuan Guo, Yehui Tang, and Enhua Wu. Vision gnn: An image is worth graph of nodes. *arXiv preprint arXiv:2206.00272*, 2022.

[14] Kai Han, Yunhe Wang, Qi Tian, Jianyuan Guo, Chunjing Xu, and Chang Xu. Ghostnet: More features from cheap operations. In *Proceedings of the IEEE/CVF conference on computer vision and pattern recognition*, pages 1580–1589, 2020.

[15] Kai Han, Yunhe Wang, Yixing Xu, Chunjing Xu, Enhua Wu, and Chang Xu. Training binary neural networks through learning with noisy supervision. In *International Conference on Machine Learning*, pages 4017–4026. PMLR, 2020.

[16] Kaiming He, Xiangyu Zhang, Shaoqing Ren, and Jian Sun. Spatial pyramid pooling in deep convolutional networks for visual recognition. *IEEE transactions on pattern analysis and machine intelligence*, 37(9):1904–1916, 2015.

[17] Kaiming He, Xiangyu Zhang, Shaoqing Ren, and Jian Sun. Deep residual learning for image recognition. In *Proceedings of the IEEE conference on computer vision and pattern recognition*, pages 770–778, 2016.

[18] Yang He, Guoliang Kang, Xuanyi Dong, Yanwei Fu, and Yi Yang. Soft filter pruning for accelerating deep convolutional neural networks. *arXiv preprint arXiv:1808.06866*, 2018.

[19] Geoffrey Hinton, Oriol Vinyals, Jeff Dean, et al. Distilling the knowledge in a neural network. *arXiv preprint arXiv:1503.02531*, 2(7), 2015.

[20] Hyungjun Kim, Jihoon Park, Changhun Lee, and Jae-Joon Kim. Improving accuracy of binary neural networks using unbalanced activation distribution. In *Proceedings of the IEEE/CVF conference on computer vision and pattern recognition*, pages 7862–7871, 2021.

[21] Alex Krizhevsky, Ilya Sutskever, and Geoffrey E Hinton. Imagenet classification with deep convolutional neural networks. *Advances in neural information processing systems*, 25, 2012.

[22] Yunqiang Li, Silvia-Laura Pintea, and Jan C van Gemert. Equal bits: Enforcing equally distributed binary network weights. In *Proceedings of the AAAI Conference on Artificial Intelligence*, volume 36, pages 1491–1499, 2022.

[23] Zhen Li, Jinglei Yang, Zheng Liu, Xiaomin Yang, Gwanggil Jeon, and Wei Wu. Feedback network for image super-resolution. In *Proceedings of the IEEE/CVF Conference on Computer Vision and Pattern Recognition*, pages 3867–3876, 2019.

[24] Dongze Lian, Zehao Yu, Xing Sun, and Shenghua Gao. As-mlp: An axial shifted mlp architecture for vision. *arXiv preprint arXiv:2107.08391*, 2021.

[25] Mingbao Lin, Rongrong Ji, Zihan Xu, Baochang Zhang, Yan Wang, Yongjian Wu, Feiyue Huang, and Chia-Wen Lin. Rotated binary neural network. *Advances in neural information processing systems*, 33:7474–7485, 2020.

[26] Xiaofan Lin, Cong Zhao, and Wei Pan. Towards accurate binary convolutional neural network. *Advances in neural information processing systems*, 30, 2017.

[27] Zechun Liu, Zhiqiang Shen, Marios Savvides, and Kwang-Ting Cheng. Reactnet: Towards precise binary neural network with generalized activation functions. In *European Conference on Computer Vision*, pages 143–159. Springer, 2020.

[28] Zechun Liu, Baoyuan Wu, Wenhan Luo, Xin Yang, Wei Liu, and Kwang-Ting Cheng. Bi-real net: Enhancing the performance of 1-bit cnns with improved representational capability and advanced training algorithm. In *Proceedings of the European conference on computer vision (ECCV)*, pages 722–737, 2018.

[29] Ilya Loshchilov and Frank Hutter. Decoupled weight decay regularization. *arXiv preprint arXiv:1711.05101*, 2017.

[30] Jian-Hao Luo, Jianxin Wu, and Weiyao Lin. Thinet: A filter level pruning method for deep neural network compression. In *Proceedings of the IEEE international conference on computer vision*, pages 5058–5066, 2017.

[31] Brais Martinez, Jing Yang, Adrian Bulat, and Georgios Tzimiropoulos. Training binary neural networks with real-to-binary convolutions. *arXiv preprint arXiv:2003.11535*, 2020.

[32] Ying Nie, Kai Han, Zhenhua Liu, An Xiao, Yiping Deng, Chunjing Xu, and Yunhe Wang. Ghostsr: Learning ghost features for efficient image super-resolution. *arXiv preprint arXiv:2101.08525*, 2021.

[33] Ying Nie, Kai Han, and Yunhe Wang. Multi-bit adaptive distillation for binary neural networks.

[34] Hyeonwoo Noh, Seunghoon Hong, and Bohyung Han. Learning deconvolution network for semantic segmentation. In *Proceedings of the IEEE international conference on computer vision*, pages 1520–1528, 2015.

[35] Mohammad Rastegari, Vicente Ordonez, Joseph Redmon, and Ali Farhadi. Xnor-net: Imagenet classification using binary convolutional neural networks. In *European conference on computer vision*, pages 525–542. Springer, 2016.

[36] Joseph Redmon, Santosh Divvala, Ross Girshick, and Ali Farhadi. You only look once: Unified, real-time object detection. In *Proceedings of the IEEE conference on computer vision and pattern recognition*, pages 779–788, 2016.

[37] Shaoqing Ren, Kaiming He, Ross Girshick, and Jian Sun. Faster r-cnn: Towards real-time object detection with region proposal networks. *Advances in neural information processing systems*, 28, 2015.

[38] Olga Russakovsky, Jia Deng, Hao Su, Jonathan Krause, Sanjeev Satheesh, Sean Ma, Zhiheng Huang, Andrej Karpathy, Aditya Khosla, Michael Bernstein, et al. Imagenet large scale visual recognition challenge. *International journal of computer vision*, 115(3):211–252, 2015.

[39] Yuzhang Shang, Dan Xu, Bin Duan, Ziliang Zong, Liqiang Nie, and Yan Yan. Lipschitz continuity retained binary neural network. In *European Conference on Computer Vision*, 2022.

[40] Karen Simonyan and Andrew Zisserman. Very deep convolutional networks for large-scale image recognition. *arXiv preprint arXiv:1409.1556*, 2014.

[41] Mingxing Tan and Quoc Le. Efficientnet: Rethinking model scaling for convolutional neural networks. In *International conference on machine learning*, pages 6105–6114. PMLR, 2019.

[42] Yehui Tang, Kai Han, Jianyuan Guo, Chang Xu, Yanxi Li, Chao Xu, and Yunhe Wang. An image patch is a wave: Phase-aware vision mlp. *arXiv preprint arXiv:2111.12294*, 2021.

[43] Yehui Tang, Yunhe Wang, Yixing Xu, Yiping Deng, Chao Xu, Dacheng Tao, and Chang Xu. Manifold regularized dynamic network pruning. In *Proceedings of the IEEE/CVF Conference on Computer Vision and Pattern Recognition*, pages 5018–5028, 2021.

[44] Yehui Tang, Yunhe Wang, Yixing Xu, Dacheng Tao, Chunjing Xu, Chao Xu, and Chang Xu. Scop: Scientific control for reliable neural network pruning. *Advances in Neural Information Processing Systems*, 33:10936–10947, 2020.

[45] Ilya O Tolstikhin, Neil Houlsby, Alexander Kolesnikov, Lucas Beyer, Xiaohua Zhai, Thomas Unterthiner, Jessica Yung, Andreas Steiner, Daniel Keysers, Jakob Uszkoreit, et al. Mlp-mixer: An all-mlp architecture for vision. *Advances in Neural Information Processing Systems*, 34, 2021.

[46] Hugo Touvron, Piotr Bojanowski, Mathilde Caron, Matthieu Cord, Alaaeldin El-Nouby, Edouard Grave, Gautier Izacard, Armand Joulin, Gabriel Synnaeve, Jakob Verbeek, et al. Resmlp: Feedforward networks for image classification with data-efficient training. *arXiv preprint arXiv:2105.03404*, 2021.

[47] Yinan Wang, Weihong "Grace" Guo, and Xiaowei Yue. Tensor decomposition to compress convolutional layers in deep learning. *IISE Transactions*, 54(5):481–495, 2022.

[48] Yixing Xu, Kai Han, Chang Xu, Yehui Tang, Chunjing Xu, and Yunhe Wang. Learning frequency domain approximation for binary neural networks. *Advances in Neural Information Processing Systems*, 34:25553–25565, 2021.

[49] Yixing Xu, Yunhe Wang, Hanting Chen, Kai Han, Chunjing Xu, Dacheng Tao, and Chang Xu. Positive-unlabeled compression on the cloud. *Advances in Neural Information Processing Systems*, 32, 2019.

[50] Yixing Xu, Chang Xu, Xinghao Chen, Wei Zhang, Chunjing Xu, and Yunhe Wang. Kernel based progressive distillation for adder neural networks. *Advances in Neural Information Processing Systems*, 33:12322–12333, 2020.

[51] Zihan Xu, Mingbao Lin, Jianzhuang Liu, Jie Chen, Ling Shao, Yue Gao, Yonghong Tian, and Rongrong Ji. Recu: Reviving the dead weights in binary neural networks. In *Proceedings of the IEEE/CVF international conference on computer vision*, pages 5198–5208, 2021.

[52] Sangdoo Yun, Dongyoon Han, Seong Joon Oh, Sanghyuk Chun, Junsuk Choe, and Youngjoon Yoo. Cutmix: Regularization strategy to train strong classifiers with localizable features. In *Proceedings of the IEEE/CVF international conference on computer vision*, pages 6023–6032, 2019.

[53] Hongyi Zhang, Moustapha Cisse, Yann N Dauphin, and David Lopez-Paz. mixup: Beyond empirical risk minimization. *arXiv preprint arXiv:1710.09412*, 2017.

[54] Wentao Zhang, Yu Shen, Zheyu Lin, Yang Li, Xiaosen Li, Wen Ouyang, Yangyu Tao, Zhi Yang, and Bin Cui. Gmlp: Building scalable and flexible graph neural networks with feature-message passing. *arXiv preprint arXiv:2104.09880*, 2021.

[55] Shuchang Zhou, Yuxin Wu, Zekun Ni, Xinyu Zhou, He Wen, and Yuheng Zou. Dorefa-net: Training low bitwidth convolutional neural networks with low bitwidth gradients. *arXiv preprint arXiv:1606.06160*, 2016.

[56] Yiren Zhou, Seyed-Mohsen Moosavi-Dezfooli, Ngai-Man Cheung, and Pascal Frossard. Adaptive quantization for deep neural network. In *Proceedings of the AAAI Conference on Artificial Intelligence*, volume 32, 2018.